Lydia-Ann L.S. Harris,[1] James R. Skinner,[1] Trevor M. Shew,[1] Terri A. Pietka,[1] Nada A. Abumrad,[1,2] and Nathan E. Wolins[1]

Perilipin 5–Driven Lipid Droplet Accumulation in Skeletal Muscle Stimulates the Expression of Fibroblast Growth Factor 21

Diabetes 2015;64:2757–2768 | DOI: 10.2337/db14-1035

Perilipin 5 (PLIN5) is a lipid droplet protein and is highly expressed in oxidative tissue. Expression of the *PLIN5* gene is regulated by peroxisome proliferator–activated receptor-α, fasting, and exercise. However, the effect of increased muscle PLIN5 expression on whole-body energy homeostasis remains unclear. To examine this, we developed a mouse line with skeletal muscle PLIN5 overexpression (MCK-Plin5). We show that MCK-Plin5 mice have increased energy metabolism and accumulate more intramyocellular triacylglycerol but have normal glucose and insulin tolerance. MCK-Plin5 mice fed high-fat chow manifest lower expression of inflammatory markers in their liver and increased expression of "browning" factors in adipose tissue. This muscle-driven phenotype is, at least in part, mediated by myokines; the MCK-Plin5 mice have 80-fold higher *FGF21* gene expression in muscle and increased serum FGF21 concentration. The increase in FGF21 occurs mainly in muscles with a predominance of fast-twitch fibers, suggesting that fiber type–specific lipid storage may be part of the mechanism conferring metabolic protection in MCK-Plin5 mice. In conclusion, upregulating the PLIN5 level in skeletal muscle drives expression of the *FGF21* gene in fast-twitch fibers and is metabolically protective. These findings provide insight into the physiology of PLIN5 and the potential contribution of its upregulation during exercise.

Cytosolic lipid droplets (LDs) are cellular warehouses for neutral lipids. Regulatory proteins and lipid-processing enzymes dynamically associate with the monolayer that surrounds the LD lipid core. These proteins are integral to the cellular metabolic response to nutrient transitions, and dysfunction of this response leads to pathology. Overconsumption increases adipose tissue lipid storage and can result in lipid deposition in other tissues such as skeletal muscle (1). Lipid accumulation in muscle positively correlates with the incidence of obesity and insulin resistance (2). Paradoxically, intramyocellular lipid is also elevated in insulin-sensitive, endurance-trained athletes (3). Why increased muscle lipid is detrimental in one condition but not the other has yet to be fully explained. Compared with untrained muscle, trained muscle contains both increased lipid content and higher concentrations of the LD protein perilipin 5 (PLIN5) (4). This increased expression of PLIN5 in muscle may have a significant role in regulating myocyte lipid hydrolysis (5) and might be protective by providing proper lipid buffering.

PLIN5 and other members of the perilipin family bind LDs and regulate lipid storage and utilization. PLIN5 is abundant in oxidative tissue, with the highest protein expression occurring in the heart (6). PLIN5 increases triacylglycerol (TAG) storage in heart and skeletal muscle (6–8), and this sequestration of lipids into LDs may be metabolically protective. Recent evidence shows that higher ceramide content—and not intramyocellular TAG—correlates best with insulin resistance in obese people (9).

Skeletal muscle, in addition to its important role in the clearance of circulating glucose and fatty acids (FAs), secretes peptides and proteins called myokines, which can regulate nutrient utilization by muscle, liver, and adipose tissue (10). In fact, many of the beneficial effects of exercise, such as increased insulin sensitivity and anti-inflammatory action, are mediated by myokines (10,11).

[1]Center for Human Nutrition, Department of Medicine, Washington University School of Medicine, St. Louis, MO

[2]Department of Cell Biology and Physiology, Washington University School of Medicine, St. Louis, MO

Corresponding author: Nathan E. Wolins, nwolins@wustl.edu.

Received 3 July 2014 and accepted 26 March 2015.

This article contains Supplementary Data online at http://diabetes.diabetesjournals.org/lookup/suppl/doi:10.2337/db14-1035/-/DC1.

Fibroblast growth factor 21 (FGF21) is a major insulin- and exercise-responsive myokine (12,13). In muscle, expression of the *FGF21* gene is activated via the phosphoinositide 3-kinase/Akt pathway (14), and a recent study showed that FGF21 is also induced by the integrated stress response in UCP1 transgenic mice (15). FGF21 secretion or administration affects substrate utilization and has pleiotropic metabolic actions in liver, muscle, and adipose tissue. Notable effects of FGF21 include enhanced insulin sensitivity, reduced hepatosteatosis, decreased body fat, and the browning of white adipose tissue (WAT) (16,17). The data in this study show that increased muscle expression of the LD-regulating protein PLIN5 stimulates expression of the *FGF21* gene in muscle and increases serum FGF21, which may target the liver and adipose tissue. Thus a novel connection is identified between PLIN5-regulated lipid storage and muscle myokine expression.

RESEARCH DESIGN AND METHODS

Generation of Muscle Creatine Kinase–Plin5-Overexpressing Mice

cDNA encoding mouse PLIN5 was inserted into an *Eco*R1 site downstream of the muscle creatine kinase (MCK) gene promoter (18). The 5′ and 3′ junctions are gggtcacc caagcttgatatcGAATTCacc***atg***gacc and **gacttc***tga*GAATTCc tgcagcccagcttgatgggtg, respectively. The bases in the resulting two *Eco*R1 sites are capitalized, bases encoding the PLIN5 protein are bolded, and the start and stop codons are italicized. The generated construct was injected into C57Bl6/JxCBA mouse embryos by Digestive Diseases Research Core Center Transgenic Mouse Facility. Embryos were implanted in pseudopregnant mice. From these offspring one line of mice with skeletal muscle–specific overexpression of Plin5 protein was identified. Animals were housed in a pathogen-free, temperature-controlled (22°C) facility and maintained on a regular 12-h light/12-h dark cycle with ad libitum access to food and water. All studies were approved by the Washington University Institutional Animal Care and Use Committee.

Exercise

Male mice (14–15 weeks old) were subjected to an exercise regimen. A treadmill was started at 5 m/min for 5 min, then the speed was increased by 2 m/min every 15 min until the mice tired (their feet hung through the bars and they withstood an electric shock for more than 10 s).

Indirect Calorimetry and Body Composition Measurements

Male mice (15 weeks old) were placed in metabolic cages (PhenoMaster; TSE Systems) and given a 3-day acclimation period. O_2 consumption and CO_2 production of mice (every 9 min per cage using TSE Systems LabMaster software version 4.8.7) were tested for 3–5 days. The respiratory exchange ratio (RER), energy metabolism, and activity were determined using LabMaster software. Body composition was assessed in live animals using the EchoMRI 3-in-1 system and software.

Diets and Glucose and Insulin Tolerance Tests

Mice (6-week-old males) were fed standard (13% fat; 62% carbohydrate; 25% protein; PicoLab 5053) or high-fat (HF) chow (60% fat; 20% carbohydrate; 20% protein; OpenSource Diet D12491) ad libitum. After 12 weeks on the HF or standard chow diet, glucose tolerance tests (GTTs) and insulin tolerance tests (ITTs) were performed (19). Food intake was monitored in these mice during the entire dietary regimen. Mice were fasted overnight (16 h) before the GTT and for 6 h before the ITT. For GTTs, the mice received intraperitoneally a 10% solution of D-glucose (1 g/kg body weight) and for ITTs, human insulin (0.75 units/kg body weight, intraperitoneal). Tail blood glucose was determined 0, 30, 60, and 120 min after each challenge (OneTouch Ultra; LifeScan).

Blood, Serum, and Tissue Collection and Analysis

Blood was collected from mice deprived of food for 4 h (basal) or 16 h (fasted). For each condition, tail blood (~100 μL) was collected in BD Microtainer serum separator tubes, spun at 2000*g* for 5 min, and the serum stored at −80°C. For tissue collection, mice were killed by CO_2 overdose after an overnight fast, and the excised tissue was frozen immediately in liquid nitrogen. TAG (Bio-Tek Synergy II plate reader, cat. nos. 464–01601, 461–09092, 461–08892), free FA (Wako Diagnostics), and cholesterol (Infinity Cholesterol Liquid Stable Reagent; Fisher Diagnostics) in serum and tissue were measured as directed by the respective suppliers. Concentrations of TAG, diacylglycerol (DAG), and ceramide in tissues also were determined using mass spectrometry, as previously described (20). Neutral lipids were extracted by hexane, and the analyses were performed on an Agilent 1100 LC system connected to an Agilent 6460 TSQ mass spectrometer operated in electrospray ionization and positive ion mode (21). FGF21 serum concentrations were determined using a Mouse/Rat FGF-21 Quantikine ELISA Kit (R&D Systems, cat no. MF2100) following the manufacturer's instructions.

Quantitative Analysis of mRNA Expression Levels

RNA was extracted using TRIzol (Invitrogen), cDNA synthesized (SuperScript VILO), and gene expression analysis performed by quantitative RT-PCR on an ABI 7500 Fast system. All reactions were normalized to the housekeeping gene *36B4*, and relative quantitation was determined using the $2^{-(\Delta Ct)}$ method.

Skeletal Muscle Fiber Isolation and Staining

Skeletal muscle was excised, placed in collagenase buffer (1 mL/50 mg tissue in DMEM, with 10% FBS, 50 mmol/L HEPES, and 2,000 units/mL collagenase II), and incubated at 37°C for 1 h while rotating at 60 rpm. Muscle pieces then were dispersed into myofibrils by forcing several times through a pipette with a 2-mm bore diameter. The tube was filled with PBS, and after approximately 20 s, the supernatant with the myofibrils was decanted. Myofibrils were allowed to settle and were fixed by adding 2% formaldehyde (2 mL/50 mg starting muscle mass). After 1 h, the myofibrils were washed with PBS, incubated

in microscopy buffer (1% BSA, 0.1 saponin, and 10 μg/mL DAPI dissolved in PBS) at room temperature with antibodies against PLIN5, then incubated overnight with BODIPY stain (D-2191 BODIPY 493/503 fluorochrome). Each incubation was followed by washing in PBS, and the last wash was removed as thoroughly as possible before resuspending the myofibrils in Elvanol for microscopy (22).

Transmission Electron Microscopy

Electron microscopy images were obtained from the Molecular Microbiology Imaging Facility. For ultrastructural analysis, samples were fixed in 2% paraformaldehyde/2.5% glutaraldehyde (Polysciences Inc.) in 100 mmol/L cacodylate buffer (pH 7.2) for 1 h at room temperature. Samples were washed in cacodylate buffer and postfixed (1 h) in 1% osmium tetroxide (Polysciences Inc.). Samples were rinsed extensively in deionized H_2O before en bloc staining (1 h) with 1% aqueous uranyl acetate (Ted Pella Inc.). After several rinses, the samples were dehydrated in a graded series of ethanol and embedded in Eponate 12 resin (Ted Pella Inc.). Sections (95 nm) (Ultracut UCT ultramicrotome; Leica Microsystems Inc.) were stained with uranyl acetate and lead citrate and viewed on a JEOL 1200 EX transmission electron microscope (JEOL USA Inc.), equipped with an 8-megapixel digital camera (Advanced Microscopy Techniques).

Preparation of Permeabilized Muscle Fibers and High-Resolution Respirometry

After excision, extensor digitorum longus (EDL) muscles were immersed in cold BIOPS (10 mmol/L EGTA, 50 mmol/L 2-[N-morpholino]ethanesulfonic acid, 0.5 mmol/L dithiothreitol, 6.56 mmol/L $MgCL_2$, 5.77 mmol/L ATP, 20 mmol/L imidazole, and 15 mmol/L phosphocreatine [pH 7.1]), and the fibers were separated on ice using two forceps and a dissection microscope. Fibers were permeabilized at 4°C for 30 min using BIOPS solution containing 50 μg/mL saponin. Then the fibers were washed for 10 min in ice-cold mitochondrial respiration solution (MIR05; 0.5 mmol/L EGTA, 3 mmol/L $MgCl_2$, 60 mmol/L K-lactobionate, 20 mmol/L taurine, 10 mmol/L KH_2PO_4, 20 mmol/L HEPES, 110 mmol/L sucrose, and 1 g/L BSA [pH 7.1]), blotted dry, weighed (3–5 mg), and placed in the Oxygraph-2k chamber (OROBOROS Instruments, Innsbruck, Austria) containing 2 mL of 37°C MIR05. To measure O_2 flux, the following substrates were added sequentially: 5 mmol/L malate, 10 mmol/L glutamate, 2.5 mmol/L ADP, 10 mmol/L succinate, three pulses of 0.5 μmol/L carbonyl cyanide 4-(trifluoromethoxy)phenylhydrazone (FCCP), 0.5 μmol/L rotenone, and 2.5 μmol/L actinomycin A. A period of stabilization followed the addition of each substrate, and oxygen flux per mass was recorded using DatLab software (OROBOROS Instruments).

Immunoblotting

Immunoblotting was done as described previously (23). Membranes were imaged using the LI-COR Odyssey system and infrared fluorescent antibodies (LI-COR Biotechnology).

Statistics

All data are expressed as means ± SEMs, with significance at $P = 0.05$. Changes in parameters of exercise capacity, body composition, substrate oxidation, and insulin and glucose tolerance were analyzed using a paired-samples Student *t* test. For feeding studies, repeated-measures ANOVA and the Tukey post hoc procedure were used to analyze changes in body weight over time between nontransgenic (NTG) and MCK-Plin5 mice. Since the data violated the assumption of sphericity, the Greenhouse-Geisser correction was applied.

RESULTS

MCK-Plin5 Mice Have Increased LDs and Intramyocellular TAG

To evaluate the effects of increased skeletal muscle PLIN5, we generated transgenic mice with muscle-specific overexpression of Plin5 cDNA (MCK-Plin5 mice). PLIN5 expression had a profound effect on overall muscle appearance; the musculature of MCK-Plin5 mice was pink, indicating increased lipid storage, compared with the red muscle of the NTG mice (Fig. 1*A*, top). Muscle PLIN5 protein (Fig. 1*A*, bottom) and mRNA expression were markedly increased above control values in the gastrocnemius, EDL, and heart of MCK-Plin5 mice, but Plin5 mRNA was not increased in the soleus and diaphragm muscles (Fig. 1*B*). Thus PLIN5 overexpression in the MCK-Plin5 mice occurred in muscle containing mostly fast-twitch fibers (gastrocnemius and EDL) and, with the exception of the heart, was not observed in muscles containing a high proportion of slow-twitch fibers (soleus and diaphragm). Physiological increases in PLIN5 protein or gene expression in fast-twitch fibers occur in conditions such as exercise (5) and prolonged fasting (Supplementary Fig. 1). Consistent with PLIN5 overexpression driving lipid accumulation (6,8), BODIPY staining of dissociated fibers from the gastrocnemius muscle revealed a marked increase in the number of LDs in MCK-Plin5 fibers compared with fibers from NTG mice (Fig. 1*C*), and costaining with antibodies against PLIN5 confirms that these structures are PLIN5-coated LDs (Fig. 1*D*). Greater PLIN5 expression increased TAG content in the EDL, gastrocnemius, and heart by two- to approximately threefold (Fig. 1*E*). Mass spectrometry analysis showed that LDs in the gastrocnemius contained significantly higher TAG but not DAG and ceramide compared with NTG muscle (Fig. 1*F*). These data indicate that overexpression pf PLIN5 in muscle drives lipid storage into PLIN5-coated droplets containing TAG. However, a robust increase in TAG also was measured in the diaphragm, where PLIN5 expression was not increased, suggesting PLIN5-independent lipid accumulation in that tissue.

MCK-Plin5 Mice Have Decreased Body Weight, Increased Oxygen Consumption, and Dependence on Carbohydrate Metabolism on a Standard Chow Diet

We monitored the weights of mice fed standard chow for 9 weeks. MCK-Plin5 mice weighed significantly less than

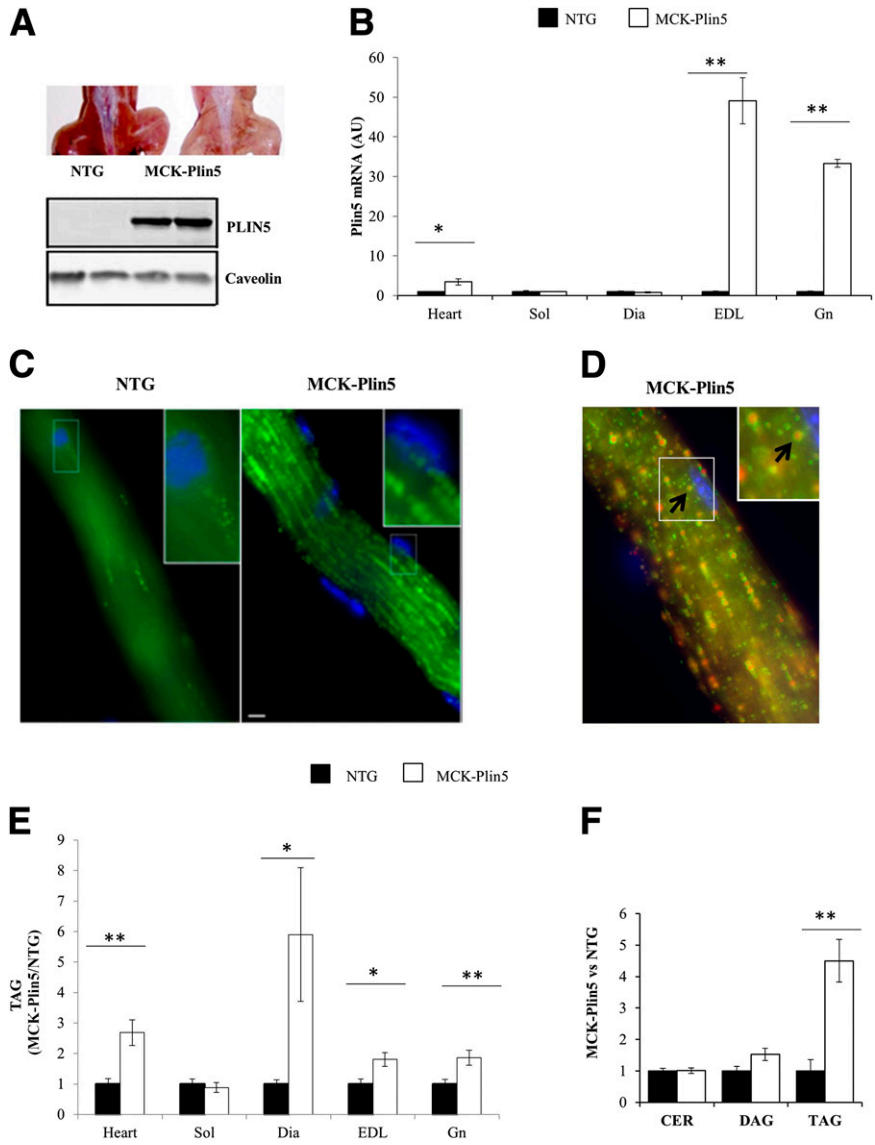

Figure 1—MCK-Plin5 mice have increased LDs and intramyocellular TAG. *A*: Top: Hindquarters of a control NTG and MCK-Plin5 mouse showing the difference in muscle color. Bottom: Western blot of gastrocnemius showing PLIN5 levels. *B*: PLIN5 mRNA expression in the heart, soleus (Sol), diaphragm (Dia), EDL, and gastrocnemius (Gn); expression was normalized to that of the housekeeping gene *36B4* (represented as arbitrary units [AUs]). *C*: Micrographs of collagenase-isolated gastrocnemius myofibrils with LDs stained with BODIPY 493/503 fluorochrome (green) and nuclei stained with DAPI (blue). *D*: Micrograph of an isolated gastrocnemius fiber. LDs are stained with BODIPY 493/503 fluorochrome (red), PLIN5 is labeled with anti-PLIN5 antibody (green), and nuclei are stained with DAPI (blue). The arrow points to a PLIN5-coated LD. *E*: Quantification of TAG content in the heart, Sol, Dia, EDL, and Gn (n = 10 mice per group). TAG levels in MCK-Plin5 muscle are expressed relative to that of NTG muscle. *F*: Mass spectrometry assessment of ceramide (CER), DAG, and TAG in gastrocnemius muscle (NTG mice, n = 4; MCK-Plin5 mice, n = 7). *$P < 0.05$; **$P < 0.01$. The data shown are representative of at least two experiments.

their NTG littermates (Fig. 2*A*), despite similar food intake (Supplementary Fig. 2) and body composition (Fig. 2*B*). Indirect calorimetric measurements showed that, compared with NTG mice, MCK-Plin5 mice had higher energy metabolism (Fig. 2*C*) and RER, especially during the dark cycle (Fig. 2*D*), without increased activity (Fig. 2*E*). These data suggest an increased dependence on carbohydrate metabolism in MCK-Plin5 mice. However, the response of MCK-Plin5 mice to an intraperitoneal bolus of glucose or insulin was similar compared with NTG mice (Fig. 2*F*). Thus PLIN5 overexpression in muscle resulted in increased TAG content and carbohydrate metabolism but had no effect on glucose and insulin tolerance or FA uptake in skeletal muscle (Table 1).

MCK-Plin5 Mice Show Evidence of Muscle Endoplasmic Reticulum Stress With No Obvious Defects in Mitochondrial or Mechanical Function

Electron microscopy examination of longitudinal slices of the gastrocnemius showed that the LDs in MCK-Plin5

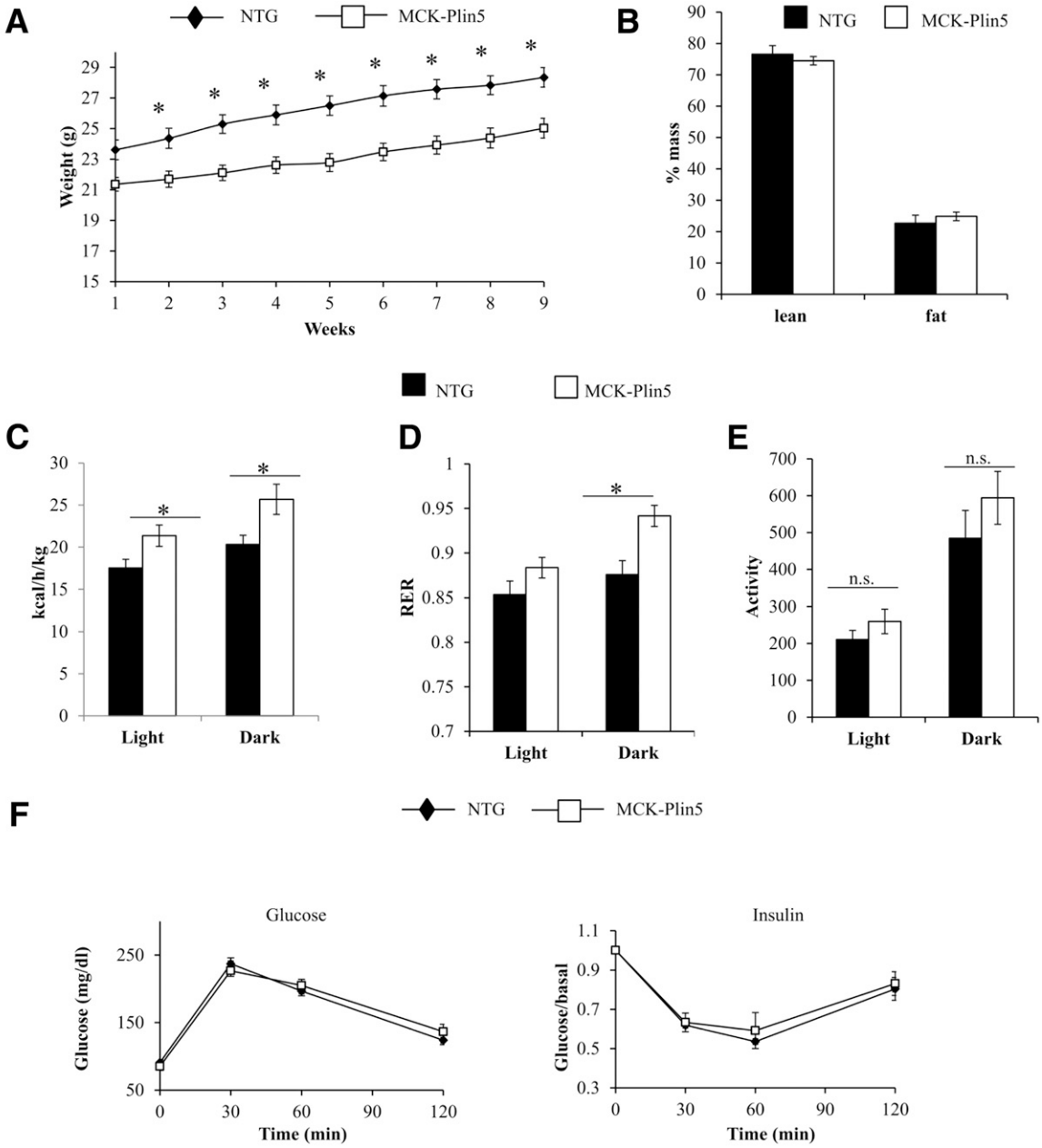

Figure 2—MCK-Plin5 mice gain less weight on a standard chow diet and have increased carbohydrate metabolism. *A*: Weight of mice on a chow diet. Mice were weighed weekly for 9 weeks (NTG mice, $n = 16$; MCK-Plin5 mice, $n = 22$). The data shown are representative of at least two experiments. *B*: Lean and fat mass expressed as a percentage of body weight ($n = 4$ mice per group). *C–E*: Energy expenditure (*C*), RER (*D*), and activity (*E*) during light and dark periods. Energy expenditure and activity were measured simultaneously (NTG mice, $n = 5$; MCK-Plin5 mice, $n = 6$). *F*: Glucose tolerance and insulin sensitivity ($n = 10$ mice per group). *$P < 0.05$.

muscle were arranged linearly and surrounded by mitochondria (Fig. 3*A*), which is a hallmark of increased PLIN5 expression (9,24). We then investigated whether PLIN5 overexpression and/or lipid accumulation affects muscle function by challenging mice with exercise. We observed no significant defect in endurance between groups (Fig. 3*B*), regardless of whether the mice were fed or fasted. High-resolution respirometry with intact muscle fibers was used to examine mitochondrial function. We detected no significant differences in the respiratory responses to glutamate, malate, ADP, succinate, FCCP, and rotenone between groups (Fig. 3*C*). This implies that the increased number of LDs and the unique organelle arrangement in transgenic mice do not affect mitochondrial usage of the substrates tested. In addition, the protein expression of mitochondrial complexes in the gastrocnemius was similar between groups (Fig. 3*D* and *E*). However, gene expression of the endoplasmic reticulum stress markers, Atf4 and Atf3 (Fig. 3*F*), and of the Atf4 targets, asparagine synthetase (Asns) and amino acid transporters

Table 1—Distribution of ^{11}C-palmitate in various tissues 20 min after venous injection (n = 4 per group)

	Injected dose/gram (%)	
Organ	NTG mice	MCK-Plin5 mice
Blood	0.95 ± 0.3	1.0 ± 0.3
Lung	10.9 ± 2.7	11.2 ± 3.8
Liver	34.0 ± 4.1	36.2 ± 5.3
Spleen	4.4 ± 0.7	6.0 ± 2.2
Kidney	13.6 ± 7.3	9.6 ± 3.5
Abdominal muscles	1.5 ± 0.6	1.8 ± 0.6
Gastrocnemius muscles	1.8 ± 0.3	1.9 ± 0.7
Fat	0.7 ± 0.4	0.7 ± 0.4
Heart	7.6 ± 1.1	14.3 ± 4.5*

Data are means ± SEMs. Animals were weighed and anesthetized with isoflurane. Approximately 50 μCi of labeled ^{11}C-palmitate in a 100-μL volume was injected into the mouse via the tail vein. Twenty minutes after injection the mice were killed and the organs were removed and placed in preweighed vials for counting (Beckman Gamma Counter). The percent of the injected dose of ^{11}C-palmitate recovered per gram organ was calculated. *$P < 0.05$.

Slc7a5 and *Slc7a11* (Fig. 3*G*), were significantly elevated in MCK-Plin5 muscle. Therefore, PLIN5 overexpression may increase endoplasmic reticulum stress while preserving mitochondrial function.

MCK-Plin5 Mice Show Decreased High-Fat Diet–Induced Weight Gain and Are Protected From Liver Inflammation

To test the metabolic flexibility of MCK-Plin5 mice, we challenged 6- to 8-week-old mice with at least 12 weeks of HF feeding. Because of the slight weight difference between transgenic and NTG mice, we weight-matched mice before administering the HF diet. Weights and food consumption were monitored during the first 9 weeks of HF feeding. MCK-Plin5 mice gained less weight than NTG mice, and the weight difference became significant after 3 weeks of HF feeding (Fig. 4*A*), which suggests that MCK-Plin5 mice are more resistant to weight gain compared with NTG mice. However, although insignificant, there was a small reduction in food consumption among HF-fed transgenic mice (Supplementary Fig. 2), which could have contributed to their decreased weight gain. Body composition and glucose and insulin tolerance did not differ between the two groups (Fig. 4*B–D*). The livers of HF-fed MCK-Plin5 mice were significantly smaller than those of their NTG littermates (Fig. 4*E*). The decreased liver weight in transgenic mice eating an HF diet was accompanied by lower liver cholesterol, whereas amount of nonesterified FAs (NEFAs) and TAG was not significantly different (Fig. 4*E*). Quantitative RT-PCR analysis revealed decreased hepatic expression of genes involved in lipid uptake (CD36, lipoprotein lipase) and FA metabolism (stearoyl-CoA desaturase 1) (Fig. 4*F*, left). Importantly, expression of several markers of macrophage infiltration and inflammation also was significantly decreased (Fig. 4*F*, right). These data show that overexpression of PLIN5 in muscle protects the liver from the negative effects of HF feeding.

FGF21 Is the Likely Mediator of Muscle and Liver Crosstalk in MCK-Plin5 Mice

Our results revealed the unexpected finding that PLIN5 overexpression in muscle had systemic effects, especially on the liver (Fig. 4 and Table 2). We therefore assessed the involvement of myokines, which usually have long-range effects on organs such as the liver and adipose tissue. We measured mRNA expression of various myokines in the gastrocnemius muscle (Fig. 5*A*) and found that only *FGF21* gene expression was significantly increased in MCK-Plin5 compared with NTG mice (Fig. 5*B*). FGF21 is an inducible secreted hormone that increases energy substrate utilization by various tissues and protects the liver from the adverse effects of HF feeding and disease (17,25). FGF21 mRNA expression was increased 80-fold in the gastrocnemius of fasting, chow-fed MCK-Plin5 mice (Fig. 5*A*). Interestingly, higher FGF21 expression was observed only in muscle rich in type II (fast-twitch) muscle fibers (gastrocnemius and EDL) and not in the heart, soleus, and diaphragm, which have abundance of type I (slow-twitch) fibers. FGF21 expression in the liver did not differ between groups. In HF-fed mice FGF21 mRNA expression also was markedly higher in the gastrocnemius and modestly higher in the epididymal WAT of MCK-Plin5 mice compared with NTG mice, whereas FGF21 expression in the liver did not differ (Fig. 5*C*). Importantly, the level of FGF21 protein was significantly elevated in the serum of fasting MCK-Plin5 mice compared with controls (Fig. 5*D*), regardless of diet. Normally, during fasting, increased serum FGF21 is primarily caused by output from the liver (25). So, to evaluate muscle contribution to serum FGF21 in MCK-Plin5 mice, we measured serum FGF21 in fed mice. Serum concentrations of FGF21 in MCK-Plin5 mice were approximately 70-fold higher than those in NTG mice, commensurate with the 80-fold increase in FGF21 expression in fasted muscle (Fig. 5*E*). These data show that MCK-Plin5 mice have chronically elevated serum FGF21, that is, under fed and fasting conditions and regardless of diet. Our data also suggests type II–rich muscle of MCK-Plin5 mice is the primary source of the observed increase in serum FGF21.

FGF21 induces "browning" of adipocytes (26). We therefore investigated the expression of various browning markers such as cell death activator A, peroxisome proliferator-activated receptor c coactivator 1-α, and CCAAT/enhancer-binding protein α in WAT. In the WAT of MCK-Plin5 mice fed a diet of standard chow, peroxisome proliferator-activated receptor c coactivator 1-α was significantly increased, whereas enhanced expression of other browning markers was observed with HF feeding (Fig. 5*F*). Therefore, enhanced browning of WAT in MCK-Plin5 mice may be

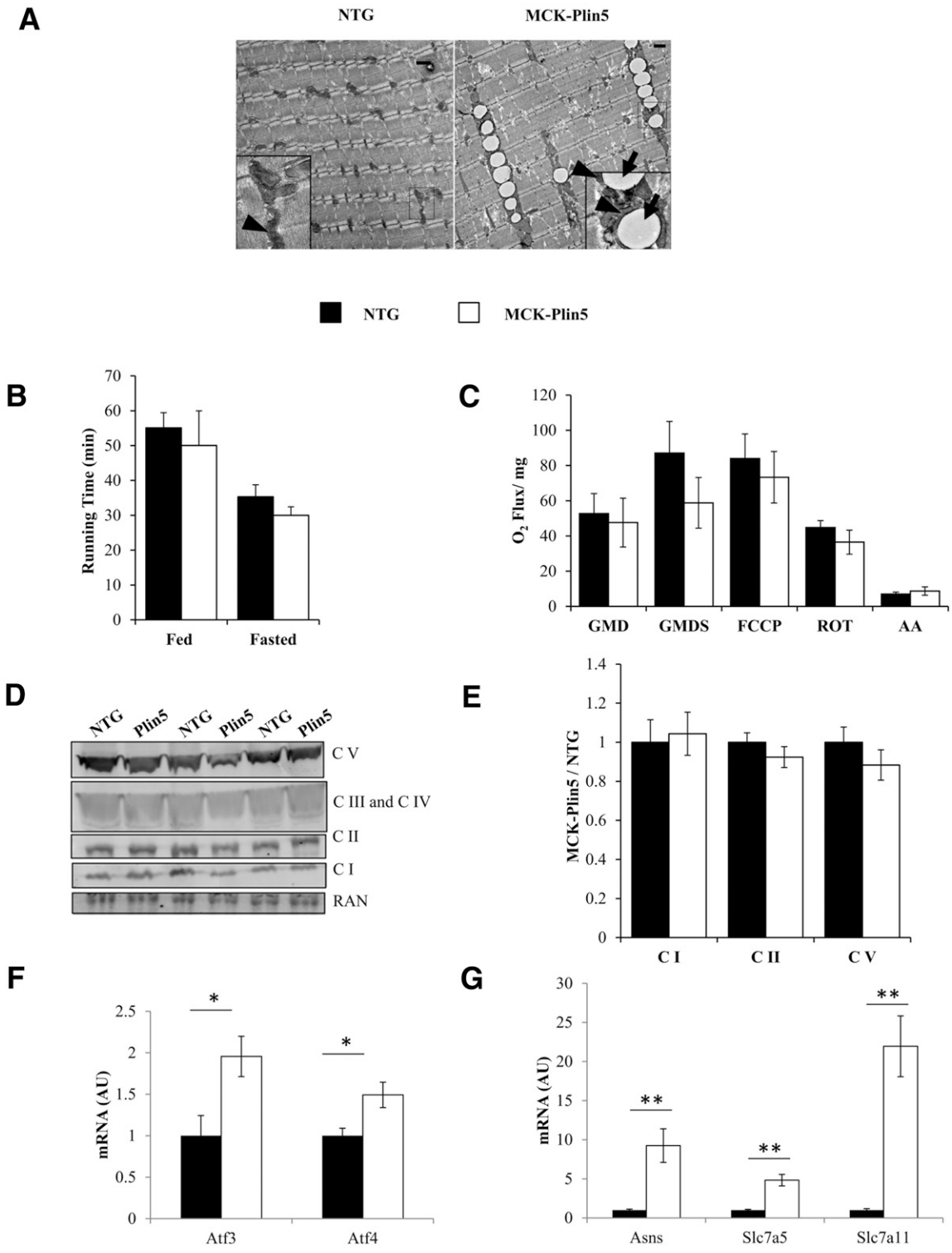

Figure 3—MCK-Plin5 mice have normal muscle function. *A*: Electron micrograph of the gastrocnemius fibers of an NTG (left) and MCK-Plin5 (right) mouse showing that mitochondria surround interfibrillar LDs in the transgenic muscle. Arrow heads show mitochondria and arrows show LDs. The data are representative of at least two experiments. *B*: Exercise endurance in NTG and MCK-Plin5 mice in the fed or fasted (16 h) state (n = 4 mice per group). *C*: Evaluation of O_2 consumption by the EDL in the presence of various substrates: malate, glutamate, ADP (GMD; complex I); malate, glutamate, ADP, succinate (GMDS; complex II); FCCP (uncoupled respiration); rotenone (ROT; complex I inhibition); and antimycin A (AA; nonmitochondria respiration) (NTG mice, n = 5; MCK-Plin5 mice, n = 6). *D*: Western blot showing the various mitochondrial protein complexes: complex I (C I), complex II (C II), complex III (C III), complex IV (C IV), complex V (C V), and Ras-related nuclear protein (RAN). *E*: Quantification of Western (n = 8 per group) signals normalized to that of RAN and compared with control. *F*: mRNA expression of *Atf3* and *Atf4* genes in the gastrocnemius. *P < 0.05. *G*: mRNA expression of ATF4 target genes in the gastrocnemius (n = 10 per group). **P < 0.01. AU, arbitrary unit.

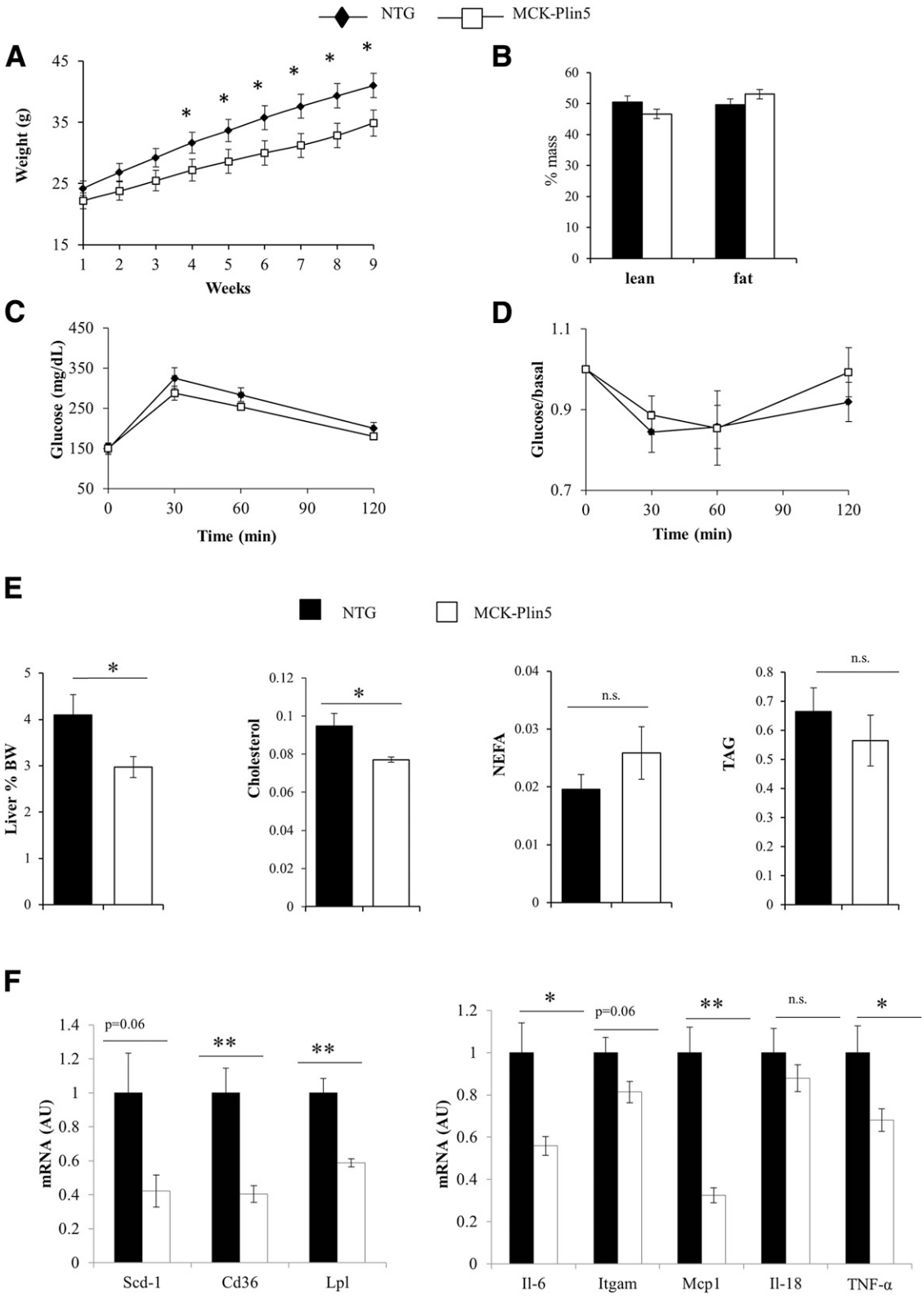

Figure 4—PLIN5 overexpression in muscle protects the liver in mice fed an HF diet. *A*: Weights of mice on an HF diet. Mice were weighed weekly for 9 weeks (NTG mice, $n = 17$; MCK-Plin5 mice, $n = 14$). *B*: Lean and fat mass as a percentage of body weight (NTG mice, $n = 4$; MCK-Plin5 mice, $n = 7$). *C*: Glucose tolerance. *D*: Insulin sensitivity. The data shown are representative of two separate experiments. *E*: Liver weights, liver cholesterol, NEFA, and TAG. Liver weight is expressed as a percentage of body weight (BW), and lipid content is normalized to milligrams protein. *F*: Quantitative RT-PCR data showing gene expression of lipid transport and metabolism genes (left) and markers of inflammation in the livers of mice fed an HF diet (right) (NTG mice, $n = 10$; MCK-Plin5 mice, $n = 9$). $^*P < 0.05$; $^{**}P < 0.01$. IL, interleukin; n.s., not significant; TNF, tumor necrosis factor.

Table 2—Serum parameters for mice fed standard and HF chow

	Standard chow		HF chow	
	NTG mice	MCK-Plin5 mice	NTG mice	MCK-Plin5 mice
Glucose (mg/dL)	169 ± 8.25	137.4 ± 6.2**	199.7 ± 15.5	192.1 ± 23.7
Glycerol (μg/μL)	0.039 ± 0.008	0.035 ± 0.005	0.029 ± 0.003	0.027 ± 0.002
TAG (μg/μL)	3.89 ± 0.52	3.39 ± 0.42	2.27 ± 0.5	1.44 ± 0.29
Cholesterol (mg/dL)	135 ± 7.4	134.6 ± 5.9	240.8 ± 12.2	205.2 ± 9.3*
NEFA (μg/μL)	0.217 ± 0.022	0.32 ± 0.023**	0.15 ± 0.021	0.12 ± 0.024

Data are means ± SEMs. Mice were fasted for 4 h in the morning before drawing blood. The glycerol, TAG, NEFA, and cholesterol content were assayed using colorimetric kits. Glucose was determined using a glucose meter before blood collection. Standard chow included $n = 10$ mice per group; HF chow included 10 NTG mice and 9 MCK-Plin5 mice. *$P < 0.05$; **$P < 0.01$.

a metabolic adaptation to dissipate excess energy on an HF diet. Together, our data suggest that FGF21 mediates the crosstalk between muscle, liver, and WAT in MCK-Plin5 mice.

DISCUSSION

PLIN5 is an LD-coating protein that can regulate both TAG storage and usage. The goal of this study was to determine the metabolic consequences of muscle-specific PLIN5 overexpression and its effects on energy regulation in response to nutritional changes.

PLIN5 overexpression via the MCK promoter occurred primarily in fast-twitch muscle and resulted in an increase in the normally low TAG content of this muscle type (Fig. 1). Muscle fiber type composition significantly influences substrate metabolism, muscle response to exercise, and the development of pathological metabolic states (27,28). PLIN5 is most highly expressed in type I–rich muscle fibers such as the heart and soleus. However, the physiological responses to exercise (5) and fasting (Supplementary Fig. 1) increase PLIN5 expression in type II muscle fibers, which suggests that PLIN5 might be part of the mechanisms underlying type II muscle adaptation to nutrient challenges. Consistent with this, MCK-Plin5 mice displayed several metabolically favorable phenotypes, such as increased energy metabolism (Fig. 3) and resistance to weight gain (Figs. 2 and 4). We also observed increased TAG content in the diaphragm and heart of MCK-Plin5 mice, despite similar or slightly increased PLIN5 expression in these tissues. This suggests some PLIN5-independent TAG accumulation. Slow-twitch muscles have increased FA uptake capacity because of the higher amounts of CD36 (29) and lipoprotein lipase (30). Thus, in the transgenic heart and diaphragm, higher serum FA (Table 2) may be the main driver of increased TAG accumulation and not PLIN5-mediated storage or lipolytic inhibition (7). It is also worth noting that while intramyocellular TAG was increased in transgenic mice, intramuscular lipid was not measured. However, body composition data suggest that these fat depots are not different between the two groups.

As shown in Table 1, we measured higher uptake of ^{11}C-palmitate in the MCK-Plin5 heart compared with the NTG heart, but this reflected only esterified palmitate and not palmitate that is oxidized by the tissue. The increased RER (Fig. 2*D*) supports the hypothesis of decreased systemic FA oxidation, which suggests that the higher FA uptake is not associated with more FA utilization.

A major finding of this study is that PLIN5 overexpression in fast-twitch muscle markedly drives expression of the *FGF21* gene (80-fold) (Fig. 5*B* and *C*) and results in chronic increases of serum FGF21. In nonfasted mice, serum FGF21 was approximately 70-fold more than that of NTG mice and paralleled the increase in muscle FGF21 mRNA expression (Fig. 5*E*). During fasting, although elevated serum FGF21 was maintained, the fold difference compared with NTG mice (Fig. 5*D*) was reduced (to twofold) because of FGF21 contributed by the liver. In the NTG mice FGF21 is produced by the liver only after a prolonged (overnight) fast. These data show that in the nonfasted MCK-Plin5 mice the muscle is the primary source of serum FGF21, whereas both muscle and liver are contributors during fasting.

Of the myokines measured, only FGF21 mRNA expression was increased in MCK-Plin5 muscle (Fig. 5*A* and *B*). Therefore, FGF21 is a likely mediator of the improved metabolic phenotype observed in the transgenic mice. There are striking similarities between the metabolic phenotypes of MCK-Plin5 mice and other mouse models of increased *FGF21* gene expression, and animals treated with exogenous FGF21 (10,15,17,31). For example, MCK-Plin5 mice have increased metabolism compared with NTG controls (Fig. 2*C–F*) and are resistant to weight gain when fed standard chow (Fig. 2*A*) or an HF diet (Fig. 4*A*). On an HF diet, MCK-Plin5 mice had lower liver cholesterol and reduced expression of lipid transport genes (Fig. 4). Resistance to weight gain and less liver fat also were observed with liver-specific FGF21 overexpression (32) and with skeletal muscle–specific deletion of Atg7, which induced FGF21 (33). Browning and reduced inflammation are documented effects of FGF21 on WAT (16). We showed increased expression of browning factors in the WAT of HF-fed MCK-Plin5 mice (Fig. 5) but did not observe changes in inflammatory markers (data not shown). Increased FGF21 expression is also a hallmark of mitochondrial deficiency or stress in mice and humans (15,33,34). However, mitochondrial function seems to be

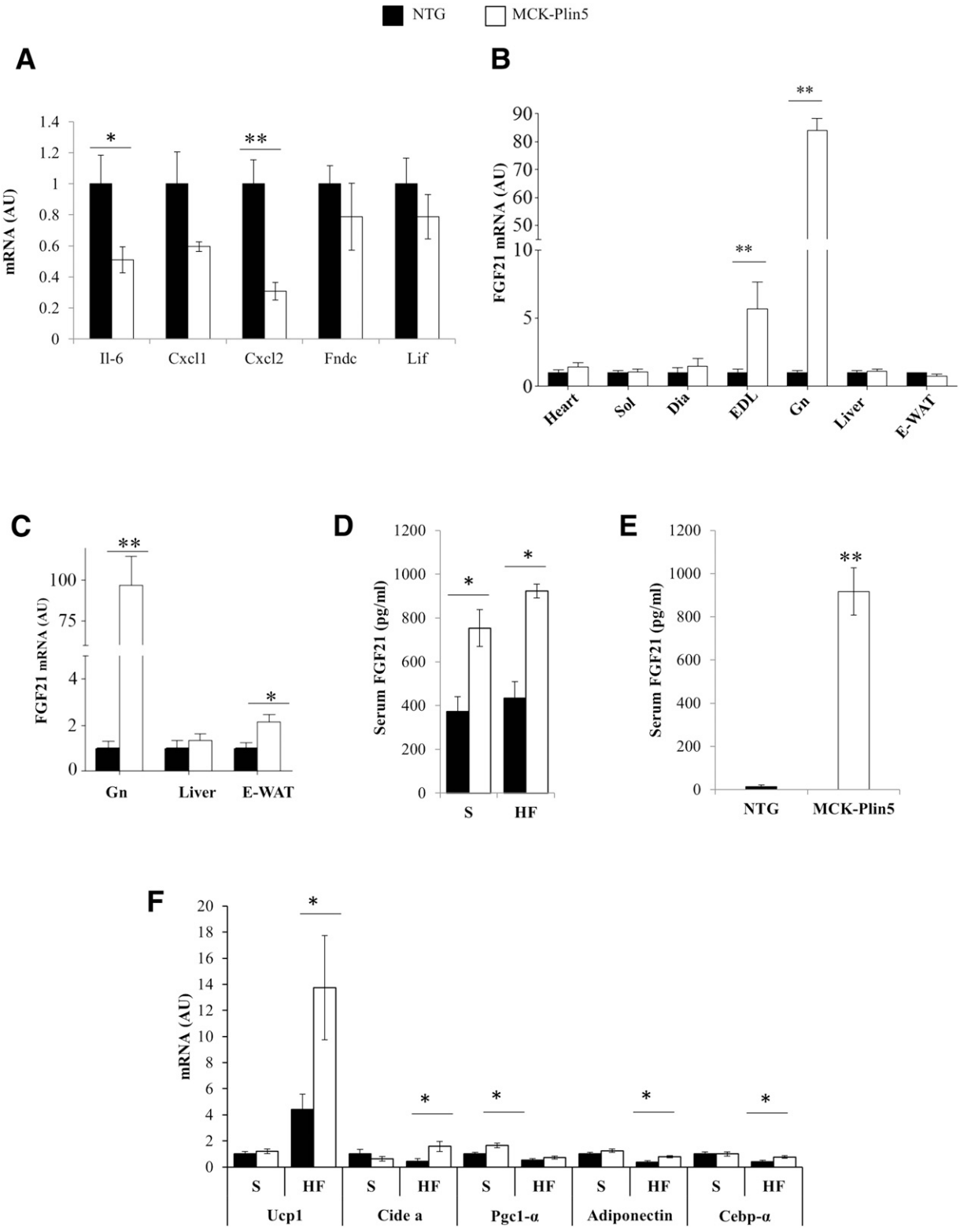

Figure 5—PLIN5 overexpression increases FGF21 expression in gastrocnemius and EDL muscles and increases FGF21 serum concentrations. *A*: mRNA expression of interleukin (Il)-6, chemokine (C-X-C motif) ligand (Cxcl) 1 and 2, fibronectin type III domain containing 5 (Fndc), and leukemia inhibitory factor (Lif) in the gastrocnemius. *B*: FGF21 mRNA expression in the heart, soleus (Sol), diaphragm (Dia), EDL, gastrocnemius (Gn), liver, and epididymal WAT (E-WAT) of mice fed standard chow. *C*: FGF21 mRNA expression in the Gn, liver, and E-WAT of mice fed a high-fat diet. *D*: Fasting serum FGF21 in mice receiving standard (S) and HF chow. *E*: Serum FGF21 in nonfasting (basal) chow-fed mice (NTG mice, $n = 4$; MCK-Plin5 mice, $n = 6$). *F*: mRNA expression of "browning" factors in the E-WAT (NTG mice, $n = 10$; MCK-Plin5 mice, $n = 9$). Except where indicated, measurements were obtained from mice fasted overnight. $^*P < 0.05$; $^{**}P < 0.01$. AU, arbitrary unit.

unaffected in MCK-Plin5 mice, probably because of the PLIN5-mediated coupling between LDs and mitochondria (Fig. 3*A*) and the funneling of TAG into LDs, which may be protective. MCK-Plin5 mice do not have increased insulin sensitivity. Therefore, PLIN5 overexpression does not enhance muscle insulin sensitivity, which is consistent with previous findings (8). FGF21 administration improves insulin sensitivity (17,35). The increased serum FGF21 in MCK-Plin5 mice did not achieve this effect, however, suggesting a threshold needed to increase insulin sensitivity or a predominance of PLIN5-mediated effects in transgenic muscle.

Together, the findings of this study suggest that elevated PLIN5 expression in type II muscle (Fig. 1*B*) may be metabolically protective. This protection seems to be partially mediated by enhanced muscle FGF21 expression, consequent to the upregulation of ATF4, which directly activates *FGF21* gene transcription (36). Chronically increased serum FGF21 in both fed and fasting mice associates with higher energy expenditure and metabolic benefits at the level of liver and adipose tissues. PLIN5 expression is usually enhanced in response to fasting and exercise in type II muscle, and our findings suggest that this adaptive change might contribute to some of the beneficial effects associated with these conditions. In addition, PLIN5-mediated TAG sequestration within LD in muscle may serve as an added metabolic benefit. This is reminiscent of the positive correlation between PLIN5 expression, increased muscle lipid, and insulin sensitivity in athletes. Thus PLIN5 expression may have a role in exercise-induced metabolic improvements.

Acknowledgments. The authors thank Gordon Smith, PhD, Center for Human Nutrition, Washington University School of Medicine, St. Louis, MO, for help with statistical analyses.

Funding. Assistance from the following core facilities at Washington University in St. Louis was provided: the Adipocyte Biology and Molecular Nutrition Core (supported by grant P30DK056341), the Digestive Diseases Research Core Center (supported by grant P30DK052574), the Nutrition Obesity Research Center (supported by grant P30DK056341 NORC), and the Mouse Cardiovascular Phenotyping Core in the Center for Cardiovascular Research and Radiological Chemistry and Imaging Laboratory. This work is supported in whole or in part by National Institutes of Health grants R01-DK088206 (to N.E.W.) and R01-DK33301 (to N.A.A.).

Duality of Interest. No potential conflicts of interest relevant to this article were reported.

Author Contributions. L.-A.L.S.H. designed the studies, collected and analyzed most of the data presented, and wrote the manuscript. J.R.S. designed the construct used to generate the MCK-Plin5 mice and helped generate preliminary data. T.M.S. provided technical assistance. T.A.P. collected and helped analyze data. N.A.A. contributed to the study direction and edited the manuscript. N.E.W. initiated the project. N.E.W. is the guarantor of this work and, as such, had full access to all the data in the study and is responsible for the integrity of the data and the accuracy of the data analysis.

References

1. Bucci M, Borra R, Någren K, et al. Human obesity is characterized by defective fat storage and enhanced muscle fatty acid oxidation, and trimetazidine gradually counteracts these abnormalities. Am J Physiol Endocrinol Metab 2011;301:E105–E112

2. Borén J, Taskinen MR, Olofsson SO, Levin M. Ectopic lipid storage and insulin resistance: a harmful relationship. J Intern Med 2013;274:25–40

3. Dubé JJ, Amati F, Stefanovic-Racic M, Toledo FG, Sauers SE, Goodpaster BH. Exercise-induced alterations in intramyocellular lipids and insulin resistance: the athlete's paradox revisited. Am J Physiol Endocrinol Metab 2008;294:E882–E888

4. Koves TR, Sparks LM, Kovalik JP, et al. PPARγ coactivator-1α contributes to exercise-induced regulation of intramuscular lipid droplet programming in mice and humans. J Lipid Res 2013;54:522–534

5. Shepherd SO, Cocks M, Tipton KD, et al. Sprint interval and traditional endurance training increase net intramuscular triglyceride breakdown and expression of perilipin 2 and 5. J Physiol 2013;591:657–675

6. Wolins NE, Quaynor BK, Skinner JR, et al. OXPAT/PAT-1 is a PPAR-induced lipid droplet protein that promotes fatty acid utilization. Diabetes 2006;55:3418–3428

7. Pollak NM, Schweiger M, Jaeger D, et al. Cardiac-specific overexpression of perilipin 5 provokes severe cardiac steatosis via the formation of a lipolytic barrier. J Lipid Res 2013;54:1092–1102

8. Bosma M, Sparks LM, Hooiveld GJ, et al. Overexpression of PLIN5 in skeletal muscle promotes oxidative gene expression and intramyocellular lipid content without compromising insulin sensitivity. Biochim Biophys Acta 2013;1831:844–852

9. Amati F, Dubé JJ, Alvarez-Carnero E, et al. Skeletal muscle triglycerides, diacylglycerols, and ceramides in insulin resistance: another paradox in endurance-trained athletes? Diabetes 2011;60:2588–2597

10. Pedersen L, Hojman P. Muscle-to-organ cross talk mediated by myokines. Adipocyte 2012;1:164–167

11. Brandt C, Pedersen BK. The role of exercise-induced myokines in muscle homeostasis and the defense against chronic diseases. J Biomed Biotechnol 2010;2010:520258

12. Kim KH, Kim SH, Min YK, Yang HM, Lee JB, Lee MS. Acute exercise induces FGF21 expression in mice and in healthy humans. PLoS One 2013;8:e63517

13. Hojman P, Pedersen M, Nielsen AR, et al. Fibroblast growth factor-21 is induced in human skeletal muscles by hyperinsulinemia. Diabetes 2009;58:2797–2801

14. Izumiya Y, Bina HA, Ouchi N, Akasaki Y, Kharitonenkov A, Walsh K. FGF21 is an Akt-regulated myokine. FEBS Lett 2008;582:3805–3810

15. Keipert S, Ost M, Johann K, et al. Skeletal muscle mitochondrial uncoupling drives endocrine cross-talk through the induction of FGF21 as a myokine. Am J Physiol Endocrinol Metab 2014;306:E469–E482

16. Fisher FM, Kleiner S, Douris N, et al. FGF21 regulates PGC-1α and browning of white adipose tissues in adaptive thermogenesis. Genes Dev 2012;26:271–281

17. Coskun T, Bina HA, Schneider MA, et al. Fibroblast growth factor 21 corrects obesity in mice. Endocrinology 2008;149:6018–6027

18. Zakeri ZF, Wolgemuth DJ, Hunt CR. Identification and sequence analysis of a new member of the mouse HSP70 gene family and characterization of its unique cellular and developmental pattern of expression in the male germ line. Mol Cell Biol 1988;8:2925–2932

19. Li B, Nolte LA, Ju JS, et al. Skeletal muscle respiratory uncoupling prevents diet-induced obesity and insulin resistance in mice. Nat Med 2000;6:1115–1120

20. Bradley D, Conte C, Mittendorfer B, et al. Gastric bypass and banding equally improve insulin sensitivity and β cell function. J Clin Invest 2012;122:4667–4674

21. Leiker TJ, Barkley RM, Murphy RC. Analysis of Diacylglycerol Molecular Species in Cellular Lipid Extracts by Normal-Phase LC-Electrospray Mass Spectrometry. Int J Mass Spectrom 2011;305:103–109

22. Harris LA, Skinner JR, Wolins NE. Imaging of neutral lipids and neutral lipid associated proteins. Methods Cell Biol 2013;116:213–226

23. Skinner JR, Shew TM, Schwartz DM, et al. Diacylglycerol enrichment of endoplasmic reticulum or lipid droplets recruits perilipin 3/TIP47 during lipid storage and mobilization. J Biol Chem 2009;284:30941–30948

24. Wang H, Sreenivasan U, Hu H, et al. Perilipin 5, a lipid droplet-associated protein, provides physical and metabolic linkage to mitochondria [published correction appears in J Lipid Res 2013;54:3539]. J Lipid Res 2011;52:2159–2168

25. Badman MK, Pissios P, Kennedy AR, Koukos G, Flier JS, Maratos-Flier E. Hepatic fibroblast growth factor 21 is regulated by PPARalpha and is a key mediator of hepatic lipid metabolism in ketotic states. Cell Metab 2007;5:426–437
26. Lo KA, Sun L. Turning WAT into BAT: a review on regulators controlling the browning of white adipocytes. Biosci Rep 2013;33:711–719
27. Gaster M, Staehr P, Beck-Nielsen H, Schrøder HD, Handberg A. GLUT4 is reduced in slow muscle fibers of type 2 diabetic patients: is insulin resistance in type 2 diabetes a slow, type 1 fiber disease? Diabetes 2001;50:1324–1329
28. Mackrell JG, Arias EB, Cartee GD. Fiber type-specific differences in glucose uptake by single fibers from skeletal muscles of 9- and 25-month-old rats. J Gerontol A Biol Sci Med Sci 2012;67:1286–1294
29. Jeppesen J, Mogensen M, Prats C, Sahlin K, Madsen K, Kiens B. FAT/CD36 is localized in sarcolemma and in vesicle-like structures in subsarcolemma regions but not in mitochondria. J Lipid Res 2010;51:1504–1512
30. Ong JM, Simsolo RB, Saghizadeh M, Pauer A, Kern PA. Expression of lipoprotein lipase in rat muscle: regulation by feeding and hypothyroidism. J Lipid Res 1994;35:1542–1551
31. Potthoff MJ, Inagaki T, Satapati S, et al. FGF21 induces PGC-1alpha and regulates carbohydrate and fatty acid metabolism during the adaptive starvation response. Proc Natl Acad Sci U S A 2009;106:10853–10858
32. Kharitonenkov A, Shiyanova TL, Koester A, et al. FGF-21 as a novel metabolic regulator. J Clin Invest 2005;115:1627–1635
33. Kim KH, Jeong YT, Oh H, et al. Autophagy deficiency leads to protection from obesity and insulin resistance by inducing Fgf21 as a mitokine. Nat Med 2013;19:83–92
34. Suomalainen A, Elo JM, Pietiläinen KH, et al. FGF-21 as a biomarker for muscle-manifesting mitochondrial respiratory chain deficiencies: a diagnostic study. Lancet Neurol 2011;10:806–818
35. Kharitonenkov A, Wroblewski VJ, Koester A, et al. The metabolic state of diabetic monkeys is regulated by fibroblast growth factor-21. Endocrinology 2007;148:774–781
36. De Sousa-Coelho AL, Marrero PF, Haro D. Activating transcription factor 4-dependent induction of FGF21 during amino acid deprivation. Biochem J 2012;443:165–171